Neutron star properties in the quark-meson coupling model

S. Pal, M. Hanauske, I. Zakout, H. Stöcker, and W. Greiner

Institut für Theoretische Physik, J.W. Goethe-Universität, D-60054 Frankfurt am Main, Germany

The effects of internal quark structure of baryons on the composition and structure of neutron star matter with hyperons are investigated in the quark-meson coupling (QMC) model. The QMC model is based on a mean-field description of nonoverlapping spherical bags bound by self-consistent exchange of scalar and vector mesons. The predictions of this model are compared with a quantum hadrodynamic (QHD) model calibrated to reproduce identical nuclear matter saturation properties. By employing a density-dependent bag constant through direct coupling to the scalar field, the QMC model is found to exhibit identical properties as QHD near saturation density. Furthermore, this modified QMC model provides well-behaved and continuous solutions at high densities relevant to the core of neutron stars. Two additional strange mesons are introduced which couple only to the strange quark in the QMC model and to the hyperons in the QHD model. The constitution and structure of stars with hyperons in the QMC and QHD models reveal interesting differences. This suggests the importance of quark structure effects in the baryons at high densities. [S0556-2813(99)03707-3]

I. INTRODUCTION

Neutron stars are born in the aftermath of supernova explosions with interior temperatures $T \gtrsim 10^{11}$ K, but cool rapidly in a few seconds by deleptonization [1] to almost cold nuclear matter. Neutron star matter is charge neutral so that gravitational force can bound it against the relatively strong repulsive Coulomb force, and is in β-equilibrium condition, i.e., in its lowest energy state. Since the matter density in the core could exceed a few times the normal nuclear matter density, neutron star matter provides an interesting possibility to investigate the strong interaction effects which are poorly understood at supernuclear density. In fact, the structure of a neutron star is chiefly determined by the equation of state (EOS) of the strongly interacting constituents.

There have been several attempts to determine the EOS for dense nucleon matter which are based primarily on nonrelativistic potential models and relativistic field theoretical models. The former approach comprises a Hamiltonian with a two-nucleon potential fitted to nucleon-nucleon scattering data and the properties of deuteron. The quantum many-body problem is traditionally handled either by a selective summation of diagrams in perturbation theory (the Brueckner-Bethe-Goldstone approach) or by using a variational method with correlation operators [2,3]. However, an important shortcoming of many potential models are that they are well suited at low densities only; the EOS becomes acausal, i.e., the speed of sound exceeds that of light at densities relevant for maximum mass neutron stars. Moreover, these models lead to symmetry energies that drastically decreases beyond about three times the saturation density which is a serious deficiency for highly asymmetric systems such as neutron stars. The alternative approach to the nuclear many body problem involves the formulation of effective relativistic field theory within the framework of quantum hadrodynamics (QHD) [4,5] where the appropriate degrees of freedom are the baryons interacting through the exchange of isoscalar scalar and vector mesons (σ, ω) and the isovector vector ρ meson which provides the driving force to the iso-

spin symmetry. The theory is an effective one since the coupling constants are determined by the saturation properties of nuclear matter. The equations of motion for the baryons and mesons are solved self-consistently in the mean field approximation. There exists a large body of calculations based on QHD which were found to provide a realistic description of bulk properties of finite nuclei and nuclear matter [4–7]. A large number of single-particle properties of finite nuclei are also well accounted including the charge distributions, spin-orbit interactions, etc. [6–10]. The central to the success of the theory is that the small binding energy in a nucleus arises from the cancelation between large Lorentz scalar and vector potentials, each of which is approximately several hundred MeV at saturation density. The potentials being comparable to the nucleon mass, it indicates the importance of relativistic effects even at normal densities. With increasing density the Fermi momentum of the baryons increases further which points to stronger relativistic effects. Therefore QHD appears to be more appropriate than nonrelativistic models for neutron star calculations. Moreover, the Lorentz covariance in this theory is retained from the outset. Consequently, the EOS automatically respect the causality limit. The relativistic mean field models with baryons and mesons as point particles, and the coupling constants determined from the saturation properties of nuclear matter, has been extrapolated into the high density regime to investigate the neutron star properties [11–15].

At high densities in the core of a neutron star the relevant degrees of freedom that may be crucial to its structure and composition are the effect of quarks confined within the hadrons. Small but interesting corrections to the standard hadronic picture have already been observed such as the EMC effect which reveals the medium modification of the internal structure of the nucleon [16]. By treating the nucleons as structureless particles, the QHD model completely misses the important effect of the constituent quarks especially at large densities. It is therefore instructive to study the relevance of the quark structure of the nucleon at supernuclear density regime as in the neutron stars. Quantum chromody-

namics (QCD) which governs the underlying strong interactions of quarks and gluons, although, believed to be essentially the fundamental theory at the nuclear and subnuclear scale is, however, intractable due to the nonperturbative features of QCD. It is therefore not a theory from which one can derive practical results for the equation of state. The most fruitful way to deal this situation would be to approach the problem from both sides, i.e., to develop the QHD and QCD motivated models and to compare their predictions.

The spontaneous symmetry breaking and chiral symmetry restoration criteria have been utilized to model effective Lagrangians for the low-energy strong interaction, such as, for example, the Nambu–Jona-Lasinio model [17]. However, these models have never been applied successfully for the description of the saturation properties of nuclear matter. On the other hand, the quark-meson coupling model proposed by Guichon [18] provides a simple and attractive framework to investigate the direct quark effects in nuclei. The model describes nuclear matter as nonoverlapping, spherical and static MIT bags in which the quarks interact through a self-consistent exchange of structureless scalar σ and vector ω mesons in the mean field approximation. This simple QMC model has been subsequently refined by including nucleon Fermi motion and center of mass corrections to the bag energy [19] and applied with reasonable success to various problems of nuclear matter [20–25] and finite nuclei [26–28]. Recently, the model has also been used to investigate the properties of Λ, Σ, and Ξ hypernuclei [29].

Although it provides a simple and interesting framework to describe the basic features of the nuclear systems in term of quark degrees freedom, the QMC model has two serious shortcomings. First, it predicts much smaller scalar and vector potentials for the nucleon than that obtained in the well-established QHD model. This implies a much smaller nucleon spin-orbit potential (sum of scalar and vector potentials) and hence weaker spin-orbit splittings in finite nuclei. Secondly, it is not apparent how far the EOS in the QMC model can be extrapolated at high densities in the neutron star interior because the assumption of nonoverlapping bags may break down. It was recently pointed out [24,25] that the small values of the nucleon potentials stem from the assumption that the bag constant is fixed at its free space value. By introducing a density-dependent bag constant (by considering it to be proportional to higher powers of the scalar field σ, for example) it was demonstrated [25] that large scalar and vector potentials are obtained. Evidently, a drop in the bag value with increasing density implies a decrease in the effective nucleon mass in a self-consistent manner. Furthermore, it was shown that the quark substructure is entirely contained in the scalar potential [20]. Therefore, the density-dependent bag constant through σ field represents, in a way, self-interaction in the scalar field in this model. This feature of nonlinear interaction in σ field, obtained by σ field-dependent bag constant may also remedy the other shortcoming of the overlapping bags at high density matter. One possible way to verify that the QMC model may be applied at supernuclear densities is by exploring observables as a function of density which shall not deviate from its continuous behavior at high densities. In other words, the QMC theory

which provides a reasonable behavior of the equation of state, etc., in the vicinity of saturation, should also be well behaved when extrapolated to supernuclear density regime. Of course, the QMC model at densities near nuclear matter value should reproduce the results based on the more established QHD model. Any deviation (not discontinuity) in the QMC results from that of the QHD at high densities may then be regarded as the effects of the quark structure beyond the structureless hadronic picture.

In this paper we shall show that by employing a bag constant coupled to the σ field, the continuity of the equation of state, etc., indeed persists in the QMC model when extrapolated to high densities relevant to the neutron star core. This will allow us to investigate the structure and composition of a neutron star in the QMC model and compare its predictions with that in the QHD model. Since the QMC model with bag constant as function of σ field represents nonlinear scalar self-interactions, for comparison we employ a QHD model which contains cubic and quartic scalar self-interactions [30]; the latter model is calibrated to reproduce the same saturation properties as the QMC model.

At high densities and hence large nucleon Fermi energies expected in the cores of stars, weak interaction energetically favor the conversion of some nucleons at the Fermi surface to hyperons. The negatively charged hyperons can then also replace the leptons. These effects cumulatively can decrease the pressure resulting in the softening of the equation of state. Within the QMC framework, only hypernuclear matter and hypernuclei [22,29] (without charge neutrality and β-equilibrium conditions) have been investigated where the bag constant is fixed to its free space value. Moreover, it was assumed [22,29] that the nonstrange σ and ω mesons couple only to the u and d quarks; the s quark is unaffected in the medium and set to its constant bare mass value. We investigate neutron star properties with an improved Lagrangian by incorporating an additional pair of hidden strange meson fields (σ^*, ϕ) which couple only to the s quark in the QMC model and only to the hyperons in the QHD model. The standard mean field model was found to be inadequate to describe the strongly attractive hyperon-hyperon interaction observed in double Λ hypernuclei [31]. The hyperon-hyperon interaction is expected to be important for hyperon rich matter [11] present in the cores of neutron stars.

The paper is organized as follows. In Sec. II, we introduce the relativistic mean field models, the QMC and the QHD, both extended to incorporate the two additional (hidden) strange mesons. The relevant equations for neutron star matter with hyperons are summarized in these models. In Sec. III, we make a systematic comparison of the QMC and the QHD results in the entire density range relevant to neutron stars. In Sec. IV, we use the model to study the constitution and structure of a star. Section V is devoted to summary and conclusions.

II. THE RELATIVISTIC MEAN FIELD MODELS

A. The extended quark-meson coupling model

In this section we present a brief introduction to the quark meson coupling model for baryonic matter and its extension

to include the hidden strange mesons which couple explicitly only to the s quark in a hyperon bag. In the QMC model, a baryon in nuclear medium is assumed to be a static spherical MIT bag in which the quarks are coupled to the meson fields in the relativistic mean field (RMF) approximation. In QMC model calculations for hadronic matter [22,29], the meson fields considered are isoscalar scalar σ and vector ω mesons and the isovector vector $\vec{\rho}^{\mu}$ meson. However, they being nonstrange are allowed to couple only to the u and d quarks within a baryon bag, while the s quark is unaffected. It is expected that with increasing density, the s quark mass should also be modified. To implement this situation, we incorporate two additional mesons, the scalar meson $f_0(m=975$ MeV$)$ (denoted as σ^* hereafter) and the vector meson $\phi(m=1020$ MeV$)$ with their masses given in the parenthesis. These strange mesons couple only to the s quark in a hyperon bag. This extended QMC model has an additional advantage that it accounts for the strongly attractive $\Lambda\Lambda$ interaction observed in hypernuclei which cannot be reproduced by (σ,ω,ρ) mesons only [31].

For a uniform static matter within the RMF, let the mean fields be denoted by σ, σ^* for the scalar mesons, and ω_0, ϕ_0 and ρ_{03} for the timelike and the isospin three-component of the vector and the vector-isovector mesons. The Dirac equation for a quark field ψ_q in a bag is then given by

$$\left[i\gamma\cdot\partial-(m_q-g_\sigma^q\sigma-g_{\sigma*}^q\sigma^*)\right.$$
$$\left.-\gamma^0\left(g_\omega^q\omega_0+g_\phi^q\phi_0+\frac{1}{2}g_\rho^q\tau_z\rho_{03}\right)\right]\psi_q=0, \quad (1)$$

where $g_\sigma^q,g_{\sigma*}^q,g_\omega^q,g_\phi^q,g_\rho^q$ are the quark-meson coupling constants and m_q the bare mass of the quark $q\equiv(u,d,s)$. The normalized ground state for a quark in a bag is given by

$$\psi_q(\mathbf{r},t)=\mathcal{N}_q\exp(-i\varepsilon_q t/R_B)\begin{pmatrix} j_0(x_q r/R_B) \\ i\beta_q\vec{\sigma}\cdot\hat{r}j_1(x_q r/R_B) \end{pmatrix}\frac{\chi_q}{\sqrt{4\pi}}, \quad (2)$$

where

$$\varepsilon_q=\Omega_q+R_B\left(g_\omega^q\omega_0+g_\phi^q\phi_0+\frac{1}{2}g_\rho^q\tau_z\rho_{03}\right),$$

$$\beta_q=\sqrt{\frac{\Omega_q-R_B m_q^*}{\Omega_q+R_B m_q^*}}. \quad (3)$$

The normalization factor is given by

$$\mathcal{N}_q^{-2}=2R_B^3 j_0^2(x_q)[\Omega_q(\Omega_q-1)+R_B m_q^*/2]/x_q^2, \quad (4)$$

with $\Omega_q=\sqrt{x_q^2+(R_B m_q^*)^2}$ the kinetic energy of the quark q and R_B is the radius of a baryon B, and χ_q the quark spinor. The effective mass of a quark is given by

$$m_q^*=m_q-g_\sigma^q\sigma-g_{\sigma*}^q\sigma^*. \quad (5)$$

The linear boundary condition, $j_0(x_q)=\beta_q j_1(x_q)$, at the bag surface determines the eigenvalue x_q.

The hyperon couplings are not relevant to the ground state properties of nuclear matter, but information about them can be available from levels in Λ hypernuclei [32]. Experimental data of Σ hypernuclei are scarce and ambiguous because of the strong $\Sigma N\rightarrow\Lambda N$ decay, while only few events in emulsion experiments with K^- beams have been attributed to the formation of Ξ^- hypernuclei. Therefore considerable uncertainty in the hyperon-nucleon interaction exists even at the normal nuclear density, their interactions at high densities are more ambiguous. In view of the uncertainties in the hyperon couplings, for simplicity, we employ in this paper the SU(6) symmetry based on the light (u,d) quark counting rule for both the scalar (σ,σ^*) and vector (ω,ϕ) coupling constants to the hyperons. The coupling constants are thus related by

$$\frac{1}{3}g_{\sigma N}=\frac{1}{2}g_{\sigma\Lambda}=\frac{1}{2}g_{\sigma\Sigma}=g_{\sigma\Xi}\equiv g_\sigma^q,$$

$$\frac{1}{3}g_{\omega N}=\frac{1}{2}g_{\omega\Lambda}=\frac{1}{2}g_{\omega\Sigma}=g_{\omega\Xi}\equiv g_\omega^q,$$

$$g_{\rho N}=\frac{1}{2}g_{\rho\Sigma}=g_{\rho\Xi}\equiv g_\rho^q, \quad g_{\rho\Lambda}=0. \quad (6)$$

The couplings to the strange mesons are

$$2g_{\sigma*\Lambda}=2g_{\sigma*\Sigma}=g_{\sigma*\Xi}=\frac{2\sqrt{2}}{3}g_{\sigma N}\equiv 2\sqrt{2}g_\sigma^q, \quad g_{\sigma*N}=0,$$

$$2g_{\phi\Lambda}=2g_{\phi\Sigma}=g_{\phi\Xi}=\frac{2\sqrt{2}}{3}g_{\omega N}\equiv 2\sqrt{2}g_\omega^q, \quad g_{\phi N}=0. \quad (7)$$

Note that in a baryon the u and d quarks are not coupled to the strange (σ^*,ϕ) mesons, i.e., $g_{\sigma*}^{u,d}=g_\phi^{u,d}=0$, while the s quark is unaffected by the (σ,ω) mesons, i.e., $g_\sigma^s=g_\omega^s=0$. Furthermore, from Eqs. (6) and (7) it is evident that the coupling constants of the s quark to (σ^*,ϕ) may be obtained from the coupling constants of the (u,d) quarks to (σ,ω) mesons by the relation $g_{\sigma*}^s=\sqrt{2}g_\sigma^{u,d}$ and $g_\phi^s=\sqrt{2}g_\omega^{u,d}$. The energy of a baryon bag consisting of three ground state quarks is then given by

$$E_B^{\text{bag}}=\frac{\displaystyle\sum_q n_q\Omega_q-z_B}{R_B}+\frac{4}{3}\pi R_B^3 B_B, \quad (8)$$

where n_q is the number of quarks of type q, z_B accounts for the zero-point motion, and B_B is the bag constant for the baryon species B. After the corrections of spurious center of mass motion, the effective mass of a baryon is given by [19,20]

TABLE I. The free space values of bag parameters z_0 and bag radii R_0 for different baryons obtained by reproducing the baryonic masses m_B in free space. The bag constant for the baryons at the free space value is $B_0^{1/4} = 188.1$ MeV while the masses of the quarks are taken as $m_u = m_d = 0$ and $m_s = 150$ MeV. The strangeness S_B of the baryons are also given.

Baryon	m_B (MeV)	S_B	z_0	R_0 (fm)
N	939	0	2.030	0.600
Λ	1116	-1	1.815	0.642
Σ	1193	-1	1.629	0.669
Ξ	1313	-2	1.505	0.686

$$m_B^* = \sqrt{(E_B^{\text{bag}})^2 - \sum_q n_q (x_q/R_B)^2}. \tag{9}$$

For fixed meson fields, the bag radius R_B is determined by the equilibrium condition of the baryon bag in the medium $\partial m_B^*/\partial R_B = 0$. For a given value of bag constant $B_B = B_0$ in free space, the parameter z_B and the bag radius R_B of the baryons may be obtained by reproducing the physical masses of the baryons, i.e., Eq. (9) in free space. In the present calculation, the current quark masses considered are $m_u = m_d = 0$ and $m_s = 150$ MeV. For our choice of free space bag constant $B_0^{1/4} = 188.1$ MeV, the values of z_B and R_B are collected in Table I. It is seen that for the fixed bag value, the equilibrium condition in free space results in an increase of the bag radius and a decrease of the zero-point motion for the heavier species.

In the original version of the QMC model [18] the bag constant was held fixed at its free space value $B = B_0$. The bag constant is a nonuniversal quantity associated with the QCD trace anomaly. When a baryonic bag is immersed in matter, it is expected to decrease from its free space value as argued in Ref. [33]. At present, however, no reliable information on the medium dependence of B_B is available on the level of QCD calculations. Effective models, such as, for example, the Nambu–Jona-Lasinio (NJL) model [17] which approximate low-energy QCD are constructed based on symmetries and symmetry breaking patterns of QCD, in particular, the chiral symmetry breaking. The concept of bag constant arises naturally in these models where its value decreases when the density of the nuclear environment is increased [34]. To reflect this physics in the QMC model, the density dependence of the bag constant for a nucleon was proposed by Jin and Jennings [25] by considering its direct coupling to the scalar mean field, i.e.,

$$B_N/B_0 = \exp[-4g_\sigma^B \sigma/m_N], \tag{10}$$

where g_σ^B is a real parameter; in this paper we shall adopt this form of exponential dependence. This direct coupling model is inspired by a NJL-type nontopological soliton model for the nucleon [35] where a scalar soliton field is responsible for the confinement of the quarks to form a nucleon. When the nucleon soliton is inserted into the nuclear environment, the scalar soliton field will interact with the scalar mean field

[36]. In fact, a similar approach is used to construct in QHD the nonlinear mean field models, where the unknown density dependence of the nuclear energy functional is parametrized by nonlinear meson-meson interactions [37,38]. The direct coupling of the bag constant to the scalar mean field σ in nucleonic medium needs to be extended for hyperons where additional scalar field σ^* is employed. To this end, we employ consistently the SU(6) symmetries for the scalar couplings of Eqs. (6) and (7). Specifically, the bag constant B_B of a baryon is directly coupled to σ and σ^* fields through the relation

$$B_B/B_0 = \exp\left\{ -4g_\sigma'^B \left[\sum_{q=u,d} n_q \sigma \right. \right.$$
$$\left. \left. + \left(3 - \sum_{q=u,d} n_q \right) \sqrt{2}\sigma^* \right] \right/ m_B \right\}, \tag{11}$$

where m_B is the bare mass of the baryon B, and for nucleonic bags $\Sigma n_q = 3$. This modeling has only one real positive parameter $g_\sigma'^B$ which for nucleon is related to g_σ^B of Eq. (10) by $g_\sigma'^B = g_\sigma^B/3$. We have refrained from using an additional parameter for coupling to the σ^* and have rather used the SU(6) symmetries because we believe that a reliable extrapolation to high densities should be based on a model having as few adjustable parameters as possible so that the model having been fitted to saturation properties of nuclear matter can be tested for its predictive power under conditions not included in the determination of the parameters. It may be also noted that in the parametrization (11), the use of free baryonic mass m_B is essential. By considering only (σ, ω, ρ) mesons in the model, we have found that this choice of B_B/B_0 results at nuclear matter density the scaling relation $\delta m_{\Lambda,\Sigma}^*/\delta m_N^* \approx 2/3$ and $\delta m_\Xi^*/\delta m_N^* \approx 1/3$, where $\delta m_B^* = m_B - m_B^*$ for the baryon B. If we now define the field-dependent σ-B coupling constant $g_{\sigma B}(\sigma)$ by

$$g_{\sigma B}(\sigma)\sigma = m_B - m_B^*(\sigma), \tag{12}$$

the same scaling relation is obtained at the nuclear matter density, i.e., $\delta m_B^*/\delta m_N^* = g_{\sigma B}(\sigma)/g_{\sigma N}(\sigma)$ are 2/3 and 1/3 for (Λ, Σ) and Ξ, respectively. This implies that the parametrization (11) in the nonstrange sector is consistent with the SU(6) symmetry employed in determining the σ-B coupling constants. In this model the baryon effective mass m_B^* and the bag constant are determined self-consistently by combining Eqs. (8), (9), and (11). In principle, the parameter z_B may also be modified in baryonic medium. However, unlike the bag constant it is not clear how z_B changes with density as it is not directly related to chiral symmetry. In this paper we assume z_B remains constant at its free space value $z_B = z_0$ as given in Table I.

The total Lagrangian density of a neutron star matter for the full baryon octet in the QMC model within RMF approximation can be written as

$$\mathcal{L}_{\mathrm{QMC}} = \sum_B \bar{\psi}_B \Bigg[i\gamma \cdot \partial - m_B^*(\sigma,\sigma^*)$$

$$- \gamma^0 \Bigg(g_{\omega B}\omega_0 + g_{\phi B}\phi_0 + \frac{1}{2} g_{\rho B}\tau_z \rho_{03} \Bigg) \Bigg] \psi_B$$

$$+ \frac{1}{2}(m_\sigma^2 \sigma^2 + m_{\sigma*}^2 \sigma^{*2} + m_\omega^2 \omega_0^2 + m_\phi^2 \phi_0^2 + m_\rho^2 \rho_{03}^2)$$

$$+ \sum_l \bar{\psi}_l (i\gamma \cdot \partial - m_l)\psi_l. \tag{13}$$

Here the sum on B is over all the charge states of the baryon octet $(p,n,\Lambda,\Sigma^+,\Sigma^0,\Sigma^-,\Xi^0,\Xi^-)$ coupled to the $\sigma,\omega,\rho,\sigma^*,\phi$ mesons. The sum on l is over the free electrons and muons (e^- and μ^-) in the star. The baryon effective mass of Eq. (9) may be expressed in terms of the field-dependent σ-B and σ^*-B coupling strengths $g_{\sigma B}(\sigma)$ and $g_{\sigma*B}(\sigma^*)$ as

$$m_B^*(\sigma,\sigma^*) = m_B - g_{\sigma B}(\sigma)\sigma - g_{\sigma*B}(\sigma^*)\sigma^*. \tag{14}$$

The dependences of the coupling strengths on the applied scalar fields must be calculated self-consistently within the quark model.

For the QMC model, the equations of motion for the meson fields in uniform static matter are given by

$$m_\sigma^2 \sigma = \sum_B g_{\sigma B} C_B(\sigma) \frac{2J_B + 1}{2\pi^2}$$

$$\times \int_0^{k_B} \frac{m_B^*(\sigma,\sigma^*)}{[k^2 + m_B^{*2}(\sigma,\sigma^*)]^{1/2}} k^2\, dk, \tag{15}$$

$$m_{\sigma*}^2 \sigma^* = \sum_B g_{\sigma*B} C_B(\sigma^*) \frac{2J_B + 1}{2\pi^2}$$

$$\times \int_0^{k_B} \frac{m_B^*(\sigma,\sigma^*)}{[k^2 + m_B^{*2}(\sigma,\sigma^*)]^{1/2}} k^2\, dk, \tag{16}$$

$$m_\omega^2 \omega_0 = \sum_B g_{\omega B}(2J_B + 1)k_B^3/(6\pi^2), \tag{17}$$

$$m_\phi^2 \phi_0 = \sum_B g_{\phi B}(2J_B + 1)k_B^3/(6\pi^2), \tag{18}$$

$$m_\rho^2 \rho_{03} = \sum_B g_{\rho B} I_{3B}(2J_B + 1)k_B^3/(6\pi^2). \tag{19}$$

In the above equations J_B and I_{3B} are the spin and the isospin projection and k_B is the Fermi momentum of the baryon species B. On the right hand sides of Eqs. (15) and (16), a new characteristic feature of QMC beyond QHD appears through the factors $C_B(\sigma)$ and $C_B(\sigma^*)$ where

$$g_{\sigma B}C_B(\sigma) = -\frac{\partial m_B^*(\sigma,\sigma^*)}{\partial \sigma}$$

$$= \sum_{q=u,d} n_q \Bigg[g_\sigma^q \frac{E_B^{\mathrm{bag}}}{m_B^*(\sigma,\sigma^*)}$$

$$\times \Bigg\{ \Bigg(1 - \frac{\Omega_q}{E_B^{\mathrm{bag}} R_B} \Bigg) S_B(\sigma) + \frac{m_q^*}{E_B^{\mathrm{bag}}} \Bigg\}$$

$$+ g_\sigma'^B \frac{E_B^{\mathrm{bag}}}{m_B^*(\sigma,\sigma^*)} \frac{16}{3}\pi R_B^3 \frac{B_B}{m_B} \Bigg], \tag{20}$$

$$g_{\sigma*B}C_B(\sigma^*) = -\frac{\partial m_B^*(\sigma,\sigma^*)}{\partial \sigma^*} = n_s g_{\sigma*}^q \frac{E_B^{\mathrm{bag}}}{m_B^*(\sigma,\sigma^*)}$$

$$\times \Bigg\{ \Bigg(1 - \frac{\Omega_s}{E_B^{\mathrm{bag}} R_B} \Bigg) S_B(\sigma^*) + \frac{m_s^*}{E_B^{\mathrm{bag}}} \Bigg\}$$

$$+ n_s g_\sigma'^B \frac{E_B^{\mathrm{bag}}}{m_B^*(\sigma,\sigma^*)} \sqrt{2}\,\frac{16}{3}\pi R_B^3 \frac{B_B}{m_B}, \tag{21}$$

where n_s ($=3 - \Sigma_{q=u,d}n_q$) is the number of s quark in the baryon. The quark scalar densities in the bag are

$$S_B(\sigma) = \int_{k_B} d\mathbf{r}\,\bar{\psi}_q \psi_q = \frac{\Omega_q/2 + R_B m_q^*(\Omega_q - 1)}{\Omega_q(\Omega_q - 1) + R_B m_q^*/2}, \quad q \equiv (u,d), \tag{22}$$

and a similar expression for $S_B(\sigma^*)$ for the contribution from the medium modification of s quark in the field σ^*. The medium dependence of the scalar densities on the bag radius was found to be rather insensitive. The last terms in Eqs. (20) and (21) originate from the density-dependent bag constants through direct coupling to the scalar fields. It is evident from Eqs. (11), (15) and (16) that an exponential dependence of the bag constant on the fields σ and σ^* introduce a nonlinear self-interaction in these fields. Moreover, the decrease of C_B with increasing density provides a new source of attraction and thereby constitutes a new saturation mechanism which is different from QHD.

For stars in which the strongly interacting particles are baryons, the composition is determined by the requirements of charge neutrality and β-equilibrium conditions under the weak processes $B_1 \to B_2 + l + \bar{\nu}_l$ and $B_2 + l \to B_1 + \nu_l$. Under the conditions that the neutrinos have left the system, the charge neutrality condition gives

$$q_{\mathrm{tot}} = \sum_B q_B(2J_B + 1)k_B^3/(6\pi^2) + \sum_{l=e,\mu} q_l k_l^3/(3\pi^2) = 0, \tag{23}$$

where q_i corresponds to the electric charge of species i. Since the time scale of a star is effectively infinite compared to the weak interaction time scale, weak interaction violate

strangeness conservation. The strangeness quantum number is therefore not conserved in a star and the net strangeness is determined by the condition of β equilibrium which for baryon B is then given by $\mu_B = b_B \mu_n - q_B \mu_e$, where μ_B is the chemical potential of baryon B and b_B its baryon number. Thus the chemical potential of any baryon can be obtained from the two independent chemical potentials μ_n and μ_e of neutron and electron. The Fermi momentum of the baryons can be obtained from the solution of the equation $\varepsilon_B(k_B) = \mu_B$, where the energy eigenvalues of the Dirac equation for the baryons are

$$\varepsilon_B(k) = \sqrt{k^2 + m_B^{*2}(\sigma, \sigma^*)} + g_{\omega B}\omega_0 + g_{\phi B}\phi_0 + g_{\rho B}I_{3B}\rho_{03}.$$
(24)

The lepton Fermi momenta are the positive real solutions of $(k_e^2 + m_e^2)^{1/2} = \mu_e$ and $(k_\mu^2 + m_\mu^2)^{1/2} = \mu_\mu = \mu_e$. The equilibrium composition of the star is obtained by solving the set of Eqs. (15)–(19) in conjunction with the charge neutrality condition (23) at a given total baryonic density $n_B = \Sigma_B b_B (2J_B + 1)k_B^3/(6\pi^2)$; the baryon effective masses are obtained self-consistently in the bag model. The total energy density and pressure including the leptons can be obtained from the grand canonical potential to be

$$\varepsilon = \frac{1}{2}m_\sigma^2\sigma^2 + \frac{1}{2}m_{\sigma*}^2\sigma^{*2} + \frac{1}{2}m_\omega^2\omega_0^2 + \frac{1}{2}m_\phi^2\phi_0^2 + \frac{1}{2}m_\rho^2\rho_{03}^2$$

$$+ \sum_B \frac{2J_B+1}{2\pi^2} \int_0^{k_B} [k^2 + m_B^{*2}(\sigma, \sigma^*)]^{1/2}k^2\, dk$$

$$+ \sum_l \frac{1}{\pi^2} \int_0^{k_l} [k^2 + m_l^2]^{1/2}k^2\, dk,$$
(25)

$$P = -\frac{1}{2}m_\sigma^2\sigma^2 - \frac{1}{2}m_{\sigma*}^2\sigma^{*2} + \frac{1}{2}m_\omega^2\omega_0^2 + \frac{1}{2}m_\phi^2\phi_0^2 + \frac{1}{2}m_\rho^2\rho_{03}^2$$

$$+ \frac{1}{3}\sum_B \frac{2J_B+1}{2\pi^2} \int_0^{k_B} \frac{k^4\, dk}{[k^2 + m_B^{*2}(\sigma, \sigma^*)]^{1/2}}$$

$$+ \frac{1}{3}\sum_l \frac{1}{\pi^2} \int_0^{k_l} \frac{k^4\, dk}{[k^2 + m_l^2]^{1/2}}.$$
(26)

To obtain the coupling constants and the parameters in the QMC model, we recall that for a fixed $B_0^{1/4} = 188.1$ MeV, the z_0 values have been adjusted to reproduce the baryon masses in free space and these are listed in Table I. For a given value of g_σ^q, once the three coupling constants $g_{\omega N}$, $g_{\rho N}$, and $g_\sigma'^B$ are adjusted, the other coupling constants of the hyperons to the meson fields can be obtained by employing the SU(6) symmetry from Eqs. (6) and (7). For this purpose, the QMC model is solved for symmetric nuclear matter, and as in Ref. [25], for a given value of $g_\sigma^q = 1$ the coupling constants $g_{\omega N}$, $g_{\rho N}$, and $g_\sigma'^B$ are adjusted to reproduce the nuclear matter binding energy $B/A = 16$ MeV at saturation density $n_0 = 0.17$ fm^{-3} and symmetry energy $a_{sym} = 32.5$ MeV. The resulting coupling constants are given

TABLE II. The coupling constants obtained in the QMC model by reproducing the saturation density $n_0 = 0.17$ fm^{-3}, the binding energy $B/A = 16$ MeV, and the symmetry energy $a_{sym} = 33.2$ MeV. The coupling constant of the scalar σ field to the bag is $g_\sigma'^B = 2.269$. The scalar coupling constant corresponds to the free space value [see Eq. (20)] while its coupling to the (u,d) quarks is taken as $g_\sigma^q = 1$. The predicted values of compressibility and effective nucleon mass at saturation are $K = 289$ MeV and $m_N^*/m_N = 0.78$. The coupling constants in the QHD model are obtained by adjusting these same five saturation properties. The meson masses are taken to be $m_\sigma = 550$ MeV, $m_\omega = 783$ MeV, and $m_\rho = 770$ MeV.

Model	$g_\sigma^2/4\pi$	$g_\omega^2/4\pi$	$g_\rho^2/4\pi$	g_2 (fm^{-1})	g_3
QMC	5.184	5.240	5.203		
QHD	5.174	5.339	5.146	12.139	48.414

in Table II. For the parametrization employed here, the predicted values of effective nucleon mass and compressibility at saturation density are $m_N^*/m_N = 0.78$ and $K = 289$ MeV. It may be worth mentioning that in order to reproduce the same saturation properties of density, binding, and symmetry energies, the coupling constants required in the original QMC model with bag fixed at $B^{1/4} \equiv B_0^{1/4} = 188.1$ MeV are $g_\sigma^2/4\pi = 20.2$, $g_\omega^2/4\pi = 1.55$, and $g_\rho^2/4\pi = 5.51$ with a relatively larger effective mass $m_N^*/m_N = 0.89$ and smaller compressibility $K = 220$ MeV. The higher effective mass and thereby smaller scalar field potential is compensated at the saturation density by a smaller vector field, i.e., a smaller coupling $g_\omega^2/4\pi$. Since at high densities the vector field dominates over the scalar, the smaller vector coupling leads to a softer EOS. The parameters obtained here are entirely from free space value and from nuclear matter at the saturation density, therefore this set can be used also in the model with the two strange mesons. In the following we refer to the model where the interaction is mediated by (σ, ω, ρ) mesons as QMCI while its extension by incorporating (σ^*, ϕ) mesons as QMCII.

B. The extended quantum hadrodynamics model

Quark meson coupling models are designed to describe both the bulk properties of nuclear systems and medium modifications of the internal structure of the baryon. Before any reliable predictions for changes due to the quark substructure can be made especially at large densities relevant to the core of neutron stars, it is important that the QMC model predicts the established results of nuclear phenomenology obtained in the quantum hadrodynamics (QHD) model near the saturation density. In QHD the relevant degrees of freedom are the structureless baryons interacting by the exchange of mesons. The direct coupling of the bag constant to the scalar field in the QMC model mimics scalar self-interaction terms. Therefore, for a consistent comparison with this QMC model, we employ a version of QHD model which contains the cubic and quartic scalar self-interactions [30]. The Lagrangian for the baryon octet in the QHD model

within the RMF approximation is similar to that of Eq. (13) for the QMC model, but for the baryonic effective mass given by

$$m_B^* = m_B - g_{\sigma B}\sigma - g_{\sigma*B}\sigma^*$$

(27)

and contains a scalar self-interaction term

$$U(\sigma) = \frac{g_2}{3}\sigma^3 + \frac{g_3}{4}\sigma^4$$

(28)

proposed by Boguta and Bodmer [30] to get a correct compressibility at saturation density. Comparing Eqs. (14) and (27), it is clear that the coupling constants in QHD are independent of the scalar field and they are determined at the saturation density. In fact it has been demonstrated [39] that QMC model is formally equivalent to the nuclear QHD model with a field-dependent scalar-nucleon coupling. The equations of motion for only the scalar meson fields of Eqs. (15) and (16) are then modified in the QHD model to

$$m_\sigma^2\sigma + \frac{\partial}{\partial\sigma}U(\sigma) = \sum_B g_{\sigma B}\frac{2J_B+1}{2\pi^2}\int_0^{k_B}\frac{m_B^*}{[k^2+m_B^{*2}]^{1/2}}k^2\,dk,$$

(29)

$$m_{\sigma*}^2\sigma^* = \sum_B g_{\sigma*B}\frac{2J_B+1}{2\pi^2}\int_0^{k_B}\frac{m_B^*}{[k^2+m_B^{*2}]^{1/2}}k^2\,dk.$$

(30)

Here nonlinear interaction only for the σ meson is employed, the interaction between the hyperons in the QHD model are through linear σ^* and ϕ mesons. The fact that all the other meson field equations are unaltered in QHD, suggests that in the QMC model the effect of the internal quark structure of a baryon enters entirely through the factor $C_B(\sigma)$ and $C_B(\sigma^*)$ as has been mentioned in Ref. [20]. The vector fields in QMC cause only a shift in the quark wave functions. The equations of motions for the meson fields in QHD are solved self-consistently in accordance with the charge neutrality and β-equilibrium conditions to obtain the composition and structure of a neutron star. The five coupling constants $g_{\sigma N}$, $g_{\omega N}$, $g_{\rho N}$, g_2 and g_3 in this model are determined by reproducing the same equilibrium properties of saturation density, binding energy, symmetry energy, effective mass and compression modulus of the QMC model; these are given in Table II. All the other coupling constants can be obtained from these couplings. The constant g_3 in the scalar field potential (28) is found positive. This avoids the fatal problem for a quantum field theory that the energy functional may be unbounded from below which leads to instabilities at high densities with large scalar fields. Hereafter we refer to the QHD model with (σ,ω,ρ) mesons as QHDI and its extension by introducing (σ^*,ϕ) mesons as QHDII.

III. RESULTS AND DISCUSSIONS

In this section we shall present results for baryonic matter in charge neutral and β-equilibrium conditions appropriate for a neutron star in the QMC and QHD models. The effec-
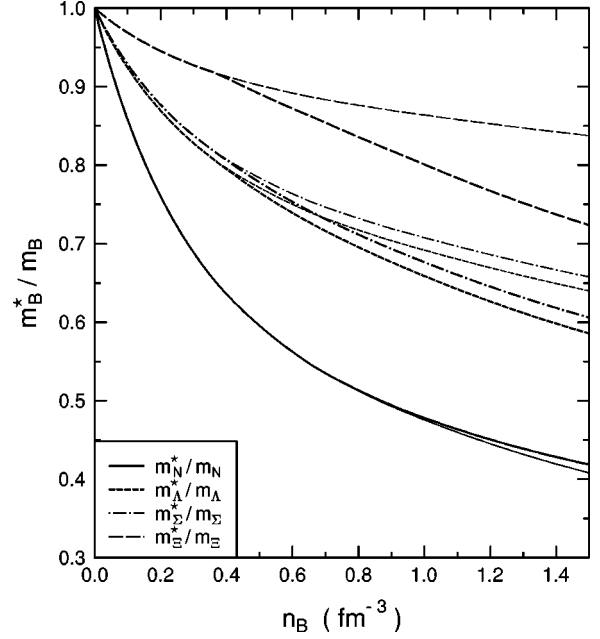

FIG. 1. The variation of effective masses m_B^*/m_B of the baryons as a function of baryon density n_B in the models QMCI (thin lines) and QMCII (thick lines).

tive baryon masses m_B^*/m_B defined in Eq. (9) are shown in Fig. 1 as a function of baryon density n_B for the models QMCI and QMCII. Unless otherwise mentioned the thin lines refer to results for different species in the model QMCI, while the thick ones correspond to those in the QMCII model. The effective masses of the nucleons rapidly decrease with increasing density and then saturate at higher densities. Since the nucleons do not couple to the strange scalar field σ^*, their masses in the models I and II are identical. At densities around nuclear matter values where hyperons have not appeared, the effective mass of a test hyperon is determined by only the scalar field σ created by nucleons which is assumed to be unaffected by inserting the hyperon. Consequently, the effective masses of all the baryons for $n_B \leq 2n_0$ reveals no splitting in models I and II. Moreover, the different baryonic masses at the saturation density indicates the SU(6) symmetry (based on the number of light quarks counting rule) for σ-B coupling, i.e., $\delta m_{\Lambda,\Sigma}^*/\delta m_N^* = 2/3$ and $\delta m_\Xi^*/\delta m_N^* = 1/3$. The QMCI model respects this scaling relation to nearly the entire density range explored here. On the other hand, in the QMCII model at densities $n_B \approx 0.38$ fm^{-3} when the hyperons (Σ^-, Λ) production threshold is reached (see Fig. 6), the attractive scalar field σ^* starts to contribute. The reduction in the mass of strange quark in model II entails a substantial decrease in the masses for the hyperons in accordance with the SU(6) relation for σ^*-B coupling. Since the Ξ hyperon has two strange quarks, its mass is maximally suppressed by the σ^* field. Note that although m_N^*/m_N reaches small values at high densities in presence of hyperons, it never becomes negative in the density range studied here. In fact, relativistic mean field models fitted to the bulk properties of nuclear matter with a high $m_N^*/m_N \approx 0.7 - 0.82$ lead to a finite effective mass even at
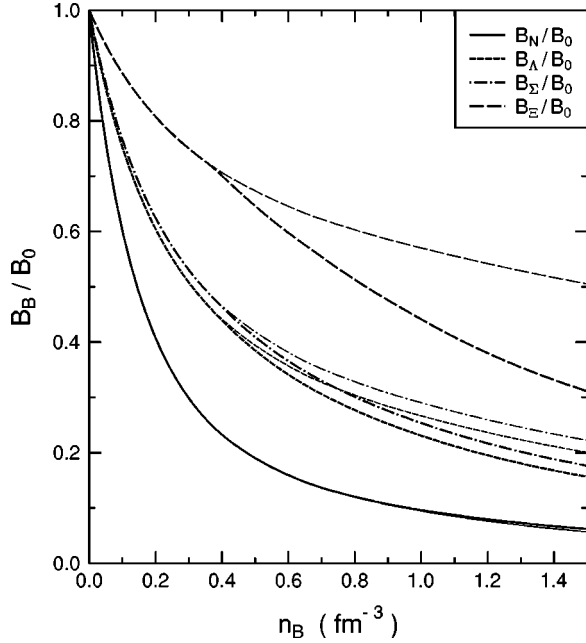
FIG. 2. The variation of bag constant B_B/B_0 of the baryons as a function of baryon density n_B in the models QMCI (thin lines) and QMCII (thick lines). The free space bag constant is taken as $B_0^{1/4} = 188.1$ MeV.
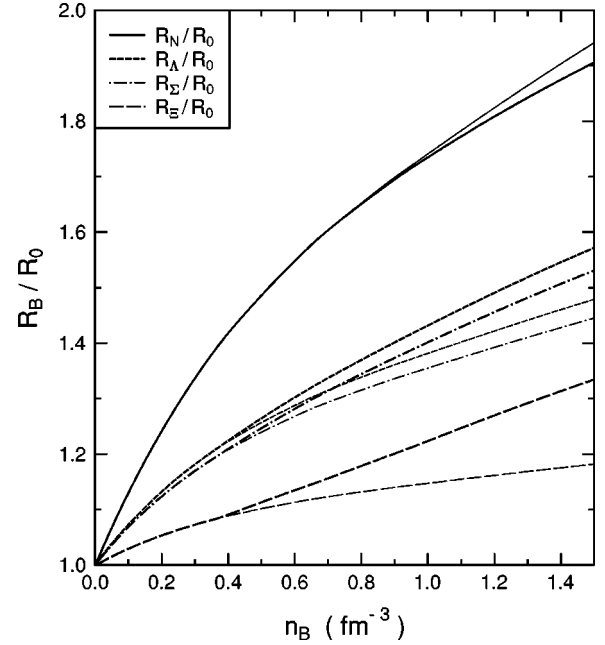

FIG. 3. The variation of bag radius R_B/R_0 of the baryons as a function of baryon density n_B in the models QMCI (thin lines) and QMCII (thick lines). The free space bag radius R_0 for different baryons are given in Table I.

central densities of maximum mass stars. However, the effective masses in this case become negative only at densities much higher than the central densities of maximum mass stars [12]. In principle parameter sets fitted to finite nuclei properties can also be obtained. However, in most of these sets the effective masses of nucleons in presence of hyperons get negative at densities much smaller than that of maximum mass stars. Therefore, these sets are not reliable to calculate neutron star properties. Recall that the original QMC model with bag constant fixed to the free space value, leads to much smaller scalar field and higher effective nucleon mass $m_N^*/m_N=0.89$. To reproduce the correct spin-orbit splitting, the reduction in the effective mass ($m_N^*/m_N=0.78$) is achieved by direct coupling of the bag constant to the scalar fields.

The variation of bag constant for the baryons B_B/B_0 [see Eq. (11)] with density is shown in Fig. 2 for the QMCI and QMCII models. The bag constants decrease with density and saturate at high densities. This behavior is similar to that of effective baryon masses as they have been obtained in a self-consistent manner. The decrease of bag constant relative to its free space value implies a decrease of bag pressure which causes an increase of bag radius in the medium. The variation of the bag radius R_B/R_0 (relative to its free space value R_0 which is different for different baryons; see Table I) with density is shown in Fig. 3. At saturation density when the bag constant for nucleon has decreased to $B_N/B_0=0.45$, the corresponding radius has increased to $R_N/R_0=1.22$. At densities of $n_B=(6-8)n_0$ corresponding to the maximum mass of neutron stars, the nucleon bag constant has decreased to a significantly small value $B_N/B_0=(0.093-0.065)$ while the corresponding radius is $75-88\%$ larger than its free space

value. This implies a considerably swollen nucleon (and hyperons) in the star matter; a detailed discussion of its consequences is given later.

We now present a systematic comparison between the QMC and the QHD models for neutron star matter with their coupling constants determined to reproduce the same set of nuclear matter saturation properties as given in Table II. In Fig. 4, the baryon effective masses m_B^*/m_B as a function of density n_B are displayed for the models QHDII (thin lines) and QMCII (thick lines). It is seen that at low and moderate densities, the m_B^*'s for the two models are in good agreement, this is not surprising as both the models are calibrated to the same properties at nuclear matter densities. At higher densities, especially when hyperons start to populate (at $n_B \approx 0.38$ fm^{-3}), the effective masses are rather distinct in the two models. The pure scalar and vector field strengths are shown in Fig. 5 as a function of density for the models QMCII (top panel) and QHDII (bottom panel). The potentials for a given baryon species are obtained by multiplying them with the corresponding coupling constants listed in Table II; for the scalar fields these couplings are however density dependent for QMCII. A careful examination of Fig. 5 indicates that the values of the fields and potentials for ω in the two models are nearly identical over the entire density range. On the other hand, at all densities the σ field in QMCII is larger than that in QHDII. However, the decreasing coupling constant $g_{\sigma N}(\sigma)$ with n_B in the former model causes the potential $U_\sigma = g_{\sigma N}(\sigma)\sigma$ to be the same as QHDII at the normal nuclear matter density. This lead to the same saturation properties (binding energy and density) in the two models. At densities higher than the normal nuclear matter value, $g_{\sigma N}(\sigma)$ further decreases causing the potential U_σ in
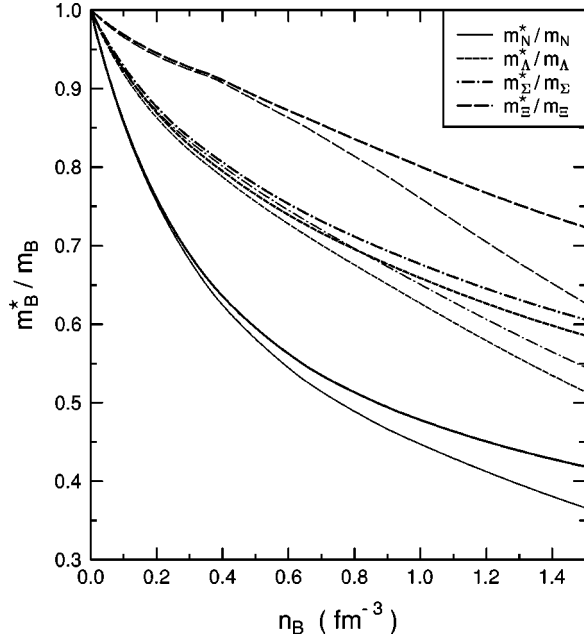
FIG. 4. The variation of effective masses m_B^*/m_B of the baryons as a function of baryon density n_B in the models QMCII (thick lines) and QHDII (thin lines).
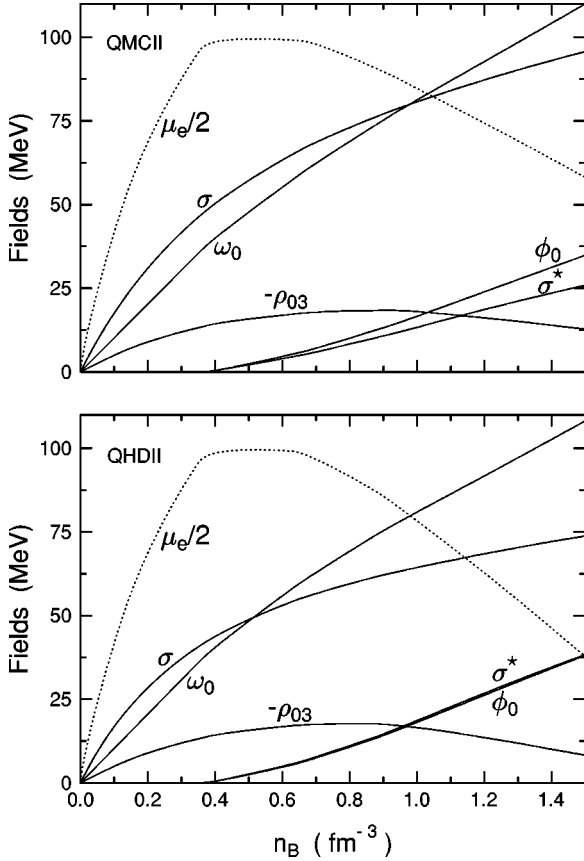

FIG. 5. The mean meson fields and the electrochemical potential versus the baryon density n_B for the models QMCII (top panel) and QHDII (bottom panel).

QMCII to saturate earlier than QHDII. In other words, the scalar density factor $C_N(\sigma)$ [see Eqs. (15) and (20)] in QMCII decreases with increasing $g_\sigma^q \sigma$ (or n_B) as quarks in the medium become more relativistic [20,29]. As a consequence, the drop in the nucleon effective mass relative to its free space value in QMCII is smaller than that in QHDII. Clearly at high densities the quark substructure of the nucleon plays a crucial role in QMC model. This feature of larger effective masses in QMCII is more evident for the hyperons. This is because of a smaller value of the attractive scalar field σ^* (see Fig. 5) and a decreasing in-medium coupling constant $g_{\sigma^* B}(\sigma^*)$ results in a much smaller potential $U_{\sigma^*} = g_{\sigma^* B}(\sigma^*)\sigma^*$ for QMCII compared to that in QHDII. The effect is most pronounced for Ξ having two strange quarks. We have observed similar qualitative differences in models I, i.e., between QMCI and QHDI. However, the distinction in m_B^* for hyperons in the two models is not so profound as they lack the σ^* meson. This indicates the importance of the strange mesons (σ^*, ϕ) which helps in revealing more clearly the quark structure of the baryons at high densities in the QMCII model as compared to the structureless baryons inherent in the QHDII model.

Having investigated the crucial role played by quarks confined within the baryons at high densities, we shall now consider whether the QMC model based on nonoverlapping bags can at all be extended to densities appropriate to neutron star interior. As is evident from Fig. 3, at rather large densities the increasing bag radius implies considerable overlapping between the bags and the nonoverlapping bag picture of nuclear matter may break down because the effects of short-range correlations among the quarks which should be associated with the overlap of hadrons are *explicitly* neglected in the quark-meson coupling model. We observe, however, that in the present QMC model the physical observables for instance the effective masses, fields and therefore the equations of state (see Fig. 7) indicate a smooth and continuous behavior from low to very high densities without any dramatic discontinuity. Any deviation at the high density regime from the QHD results may be interpreted as the interesting effects due to quark structure of the baryons only. This is in consonance with the argument put forward [40] that the physical observables do not depend on the bag radius. On contrary, in the original QMC model with bag fixed at the free space value, the observables were found [39] to differ drastically from QHD results with large discontinuities. Moreover, solutions in that version of QMC model cease to exist above $n_B \approx 4.92 n_0$ since the eigenvalue x_q in Eq. (2) vanishes. This indicates that by using a density-dependent bag constant through direct coupling to the scalar field, the QMC model not only reproduces the correct spin-orbit potential but possibly also includes the effects of quark-quark correlations associated with overlapping bags which was missing in the original QMC model. A possible explanation to this may follow from an alternative approach inspired by effective field theories. In this theory the constraint of renormalizability of the hadronic Lagrangian is abandoned [37,38] which allows to introduce higher order meson self-interaction (i.e., orders higher than the quartic scalar interaction) consistent with the underlying symmetries of QCD. By a suitable trun-

cation at some low orders of the fields, it was argued [37] that by allowing nonlinearities in the meson fields that generate additional density dependence in the interactions, the important effects of correlations (and exchange) between the nucleons beyond the simple Hartree contributions are automatically included. Thus, one can include many body effects beyond the simple Hartree level even though only classical meson fields and local interactions are retained.

In the context of QMC model, as demonstrated in this paper and also in Ref. [39], an exponential dependence of bag constant B_B on σ (and σ^*) is equivalent to scalar self-interactions of infinite orders, of course each term is smaller by a factor $\sim (g_\omega'^B/m_B)$ than its preceding one [see Eq. (11)]. Hence these higher order self-interaction terms possibly include (implicitly) the effects of quark-quark correlations at high densities providing a nondiscontinuity in the physical observables, unlike the original version of the QMC model with constant bag. This suggests that in a QMC model with bag constant coupled to the scalar field, one can in principle extrapolate to high densities to explore the neutron star properties.

IV. COMPOSITION AND STRUCTURE OF NEUTRON STAR MATTER

In this section the constitution and structure of stable charge neutral (neutron star) matter in the supernuclear density regime are presented in the QMC and QHD models. In Fig. 6 the abundances of baryons and leptons as a function of density in the star matter are shown for the models QMCII (top panel) and QHDII (bottom panel). At densities slightly below the nuclear matter value, the β decay of neutrons to muons are allowed, and thus muons start to populate. The charge neutrality of a star forces a high isospin asymmetry so both the electron chemical potential μ_e and the ρ field, ρ_{03}, grow at low density as evident from Fig. 5. Although the ρ field is very small and never exceeds -18 MeV, its correct determination from symmetry energy is of utmost importance as it determines the proton fraction. It was demonstrated [41] that for a npe system rapid cooling by nucleon direct URCA process is allowed by the momentum conservation condition $k_p + k_e \geq k_n$ which corresponds to a proton fraction $Y_p \gtrsim 0.11$. In both the models used here this condition is satisfied at densities $n_B \gtrsim 0.28$ fm^{-3} thus rapid cooling by direct URCA process can occur. In the absence of any hyperons, the charge neutrality condition forces the proton (and lepton) fractions to continuously increase with density in these relativistic mean field models. Thus once the threshold density for cooling by direct URCA process is achieved, it would persist up to the center of such stars. In contrast, the decreasing symmetry energy at high densities in the nonrelativistic models would limit cooling near the central region of massive stars. The symmetry energy also determines the hyperon production threshold density obtained by the condition $\mu_B = \mu_n - q_B \mu_e \geq \varepsilon_B(k=0)$, where the energy eigenvalue ε_B is given by Eq. (24). Consequently the threshold density for a hyperon species is determined by its charge and effective mass and by all the fields present in the system. As expected, the Λ with mass 1116 MeV and Σ^- with a mass
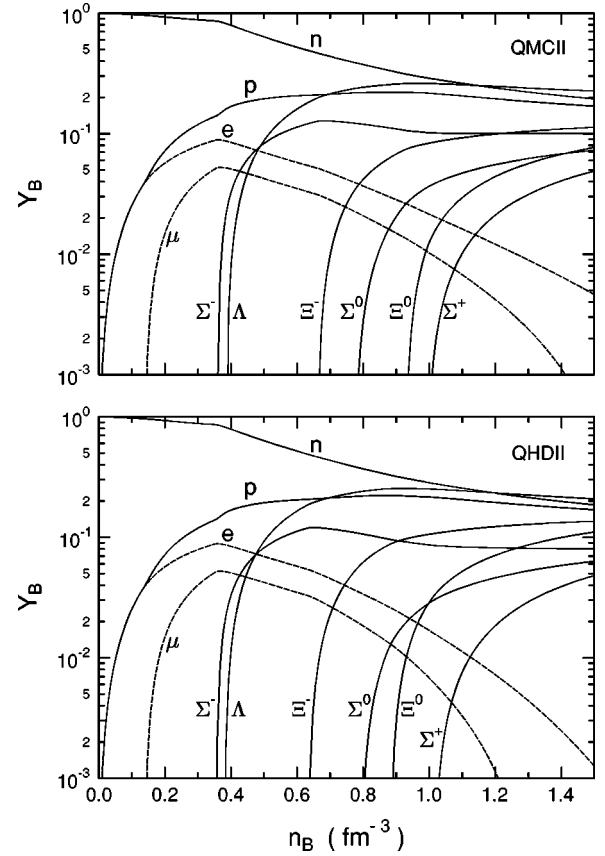

FIG. 6. The composition of neutron star matter with hyperons in the models QMCII (top panel) and QHDII (bottom panel).

1193 MeV appear at roughly the same density $n_B \approx 0.38$ fm^{-3}, because the somewhat larger mass of Σ^- is compensated by its negative charge. Since charge neutrality can now occur more economically by Σ^-, the lepton fraction begins to fall. The electron chemical potential (see Fig. 5) then saturates around 200 MeV and subsequently decreases with increasing Σ^- population. More massive and positively charged particles than these appear at high densities. The substantial reduction in the effective mass of Ξ in QHDII (as shown in Fig. 4) is manifested by a relatively early appearance of Ξ^- and Ξ^0 and their larger abundances in the star compared to that in QMCII. The enhanced Ξ^- production in turn causes a further rapid decrease of the lepton fraction in QHDII. At high densities, all the baryons tend to saturate with the abundance of Λ being maximum, even exceeding the number of neutrons. Because of the fast growth of the hyperons and their comparable abundances with the nucleons, the dense interior of a star resembles more a hyperon star than a neutron star. The net strangeness fraction for stars in the model QHDII is slightly enhanced due to larger Ξ abundance than that in QMCII. In contrast to pure npe stars, the proton fraction here reaches maximum value once the hyperons (Σ, Λ) start populating and thereafter it saturates at the level of 20%. Therefore rapid cooling by nucleon direct URCA process can still occur in these stars. Since the critical density of nucleon direct URCA process is nearly identical to the hyperon threshold density, and the emmisivities from the
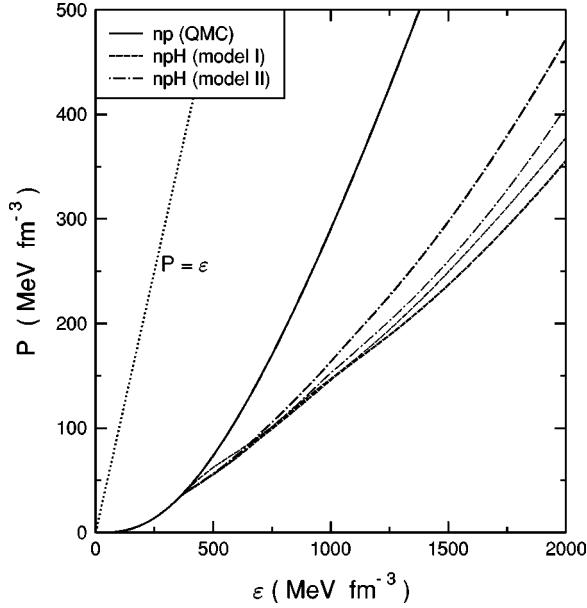
FIG. 7. The equation of state, pressure P vs energy density ε for nucleons only (np) star (solid line) in the QMC model, and for stars with further inclusion of hyperons (npH) in models I (dashed lines) and in models II (dash-dotted) lines. The results are for QMC models (thick lines) and QHD models (thin lines). The causal limit ($P=\varepsilon$) is also shown.

FIG. 8. The adiabatic index Γ vs the energy density ε for nucleons only (np) star (solid lines), and for stars with further inclusion of hyperons (npH) in models I (dashed lines) and in models II (dash-dotted lines). The results are for QMC models (thick lines) and QHD models (thin lines).

hyperon direct URCA processes are about 5–100 times smaller than that from the nucleons [42], the stars cooling by direct URCA process is dominated by nucleons—the hyperons would only have a minor contribution to it. In the models QMCI and QHDI, the effective masses of the hyperons and the potentials are, however, found to be almost identical, hence the composition of the stars in model I were found to be practically indistinguishable.

The equation of state, pressure P versus the energy density ε is displayed in Fig. 7 for the different models studied here. The EOS for nucleons only (np) star shown for the QMC model (solid line) is found to be considerably stiff. Since the corresponding EOS in the QHD model is found to be nearly identical we do not present the result for clarity. At high densities when the Fermi energy of nucleons exceeds the effective mass of hyperons minus their associated interaction energy, the conversion of nucleons to hyperons is energetically favorable. Since this conversion relieves the Fermi pressure of the nucleons, the equation of state is softened. This effect is further accentuated by the decrease of the pressure exerted by leptons because of their replacement by negatively charged hyperons in maintaining charge neutrality more efficiently. The EOS for nucleons plus hyperons (npH) system for both the models I and II are shown in the figure; the thick lines refer to QMC results while the thin lines correspond to QHD. Several structures observed in the equation of state correspond to the densities at which different hyperon species begins to populate. In model I (shown by dashed lines), the EOS in QMCI is found to be softer compared to QHDI. In this situation the vector fields (ω, ρ) and the effective hyperon masses are found to be same in the two models, only the scalar field σ and the effective mass of
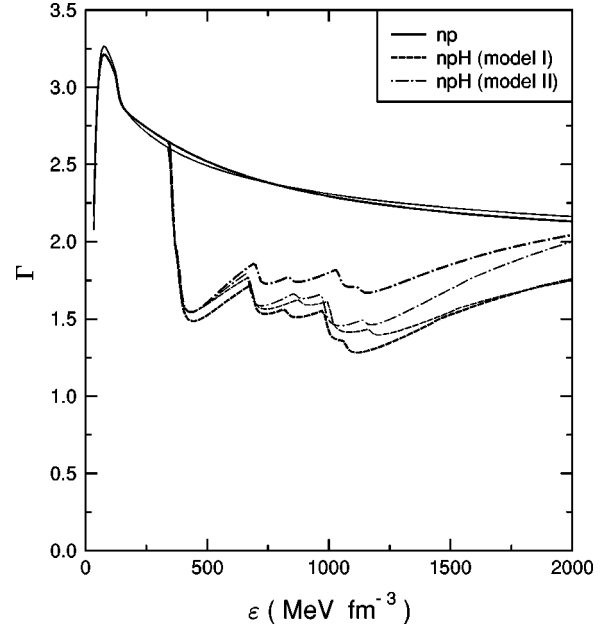
nucleons in QMCI is somewhat larger than QHDI. This results in the QMCI a larger contribution from the scalar attraction and a smaller one from the repulsive kinetic term of nucleons to the pressure [Eq. (26)] leading to a softened EOS. With the inclusion of strange mesons, the effective masses of hyperons also undergo significant reduction (see Fig. 1) while, in general, the contribution from the repulsive ϕ field dominates over the attraction from σ^* field. The net effect is thus a stiffer EOS in model II (shown by dash-dotted lines) in contrast to model I. As evident from Figs. 4 and 5, the combined effects of enhanced effective masses, considerably large repulsive ϕ field and smaller attraction from σ^* field act in increasing the pressure in QMCII compared to QHDII. This entails a pronounced stiffening with the EOS for QMCII being even stiffer relative to QHDII. Thus by including the strange mesons, a complete reversal in behavior occurs for the equation of state in QMC and QHD models which should have a significant bearing on the structure of the stars. For comparison, the causal limit $p=\varepsilon$ is also shown in the figure. All the relativistic models studies here respect causality condition $\partial p/\partial \varepsilon \lesssim 1$ so that the speed of sound remains lower than the speed of light.

An important parameter describing the equations of state is the adiabatic index $\Gamma = d\ln P/d\ln n_B = (P+\varepsilon)/P \cdot dP/d\varepsilon$. In Newtonian theory it is possible to find a stable hydrostatic configuration for a spherical mass distribution if the adiabatic index exceeds 4/3 [43], and when general relativity is included it slightly exceeds this value [44]. Figure 8 shows the adiabatic index Γ versus the energy density ε for different equations of state. At densities below the nuclear matter value, Γ could have very small values since most of the pressure support for the star originates from the electrons, the
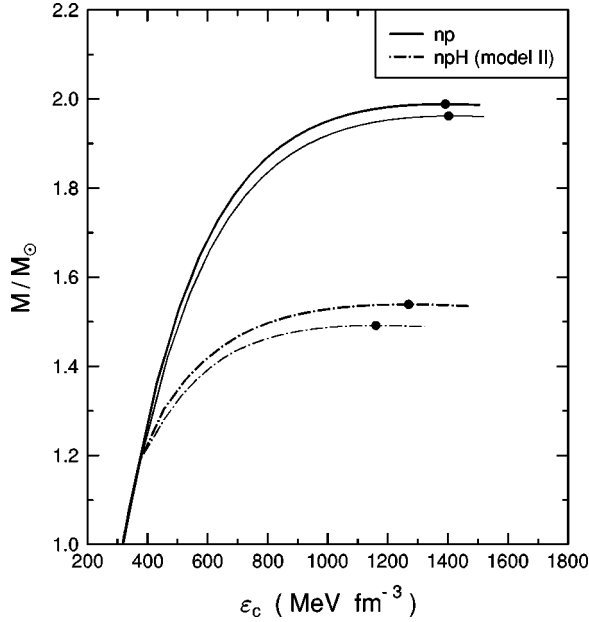
FIG. 9. The neutron star sequences near the limiting mass for nucleons only (np) star (solid lines) and for stars with further inclusion of hyperons (npH) in the model II (dash-dotted lines). The results are for the models QMC (thick lines) and QHD (thin lines). The filled circles correspond to the maximum masses.

nuclear phase has a negative contribution to pressure. At densities greater than about n_0, the EOS stiffens and Γ is significantly greater than 4/3. With the appearance of hyperons, the softening of the EOS is manifested by the considerable lowering of the adiabatic index. The several structures observed in the EOS corresponding to the population of hyperons at the threshold densities is clearly evident in Fig. 8. The adiabatic index drops at each density when a new hyperon species is populated.

The differences in the EOS at high densities are expected to be reflected in the structure of the neutron stars, namely, their masses and radii. The static neutron star sequences representing the stellar masses $M/M_\odot$ and the corresponding central energy densities ε_c obtained by solving the Tolman-Oppenheimer-Volkoff equations [45] are shown in Fig. 9 for different equations of state. In general, such a sequence possesses a minimum mass below which gravitational attraction is

not sufficient against the radial oscillations that destroy these configurations by dispersal. On the other hand, a maximum mass of the sequence exits beyond which the pressure support from the EOS is insufficient against the strong gravitational attraction. Stars beyond this mass are unstable to acoustical radial vibrations and thereby collapse to a black hole. The crustal region has a negligible contribution ($\sim 10^{-5} M_\odot$) to the total mass of a star, while most of the mass originates from the dense interior beyond the saturation density. Thus mass measurements may provide considerable insight into the interior constitution of a star. For the np system, the extremely stiff EOS corresponds to a large Fermi pressure and hence can sustain large limiting mass. The maximum masses for such np stars in the QMC model is $M_{max} = 1.988 M_\odot$, while a relatively softer EOS in the corresponding QHD model results in $M_{max} = 1.962 M_\odot$. In Table III, the maximum masses and the corresponding radii $R_{M_{max}}$ and central baryonic densities n_c are presented. In Fig. 10, we also show the mass-radius relationship of the different EOS. With the inclusion of more baryon species in the form of hyperons, the considerable softening of the EOS results in relatively much smaller mass stars. Since the QMCI model has a much softer EOS than QHDI, the M_{max} values are $1.478 M_\odot$ and $1.488 M_\odot$, respectively; the star sequence and the mass-radius relationship in these models are not shown in the figures for clarity. The larger radii obtained in stars with hyperonization are a consequence of weaker gravitational attraction from the smaller masses that causes the stars to be large and diffuse. Compared to the mass of a star where the contribution is primarily from beyond the saturation density, about 40% of the star's radius originates from the EOS at $n_B \lesssim n_0$. Consequently, radius measurements should be rather insensitive to the changes in the EOS due to quark structure of baryons or to the interior constitution of the star. In fact, no precise radius measurements currently exist. The star sequences and the mass-radius relationships in model II are shown in Figs. 9 and 10, respectively. The reversal in behavior observed in the EOS with the addition of strange mesons, i.e., the EOS is stiffer in QMCII than QHDII, is manifested in the maximum masses and the corresponding radii for such stars. For all the cases studied here, the maximum masses of the stars are found to be larger than the current observational lower limit of

TABLE III. The maximum masses $M_{max}/M_\odot$ of nonrotating stars and their corresponding radii $R_{M_{max}}$ and central densities n_c in the models QMC and QHD. The Keplerian frequency Ω_{max} for the respective rotating configurations are obtained from the relation $\Omega_{max} = 7750 (M_{max}/M_\odot)^{1/2} (R_{M_{max}}/10 \text{ km})^{-3/2} \text{ s}^{-1}$. Results are for stars with only nucleons (np); stars with further inclusion of hyperons (npH) in the model I where the interaction is mediated by (σ, ω, ρ) mesons, and stars in model II where the additional mesons (σ^*, ϕ) are included.

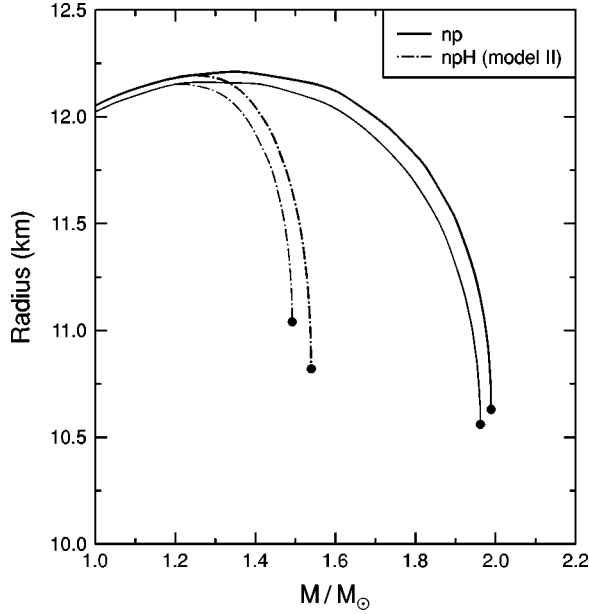|	QMC				QHD			
	$M_{max}/M_\odot$	$R_{M_{max}}$ (km)	n_c (fm^{-3})	Ω_{max} (10^3 s^{-1})	$M_{max}/M_\odot$	$R_{M_{max}}$ (km)	n_c (fm^{-3})	Ω_{max} (10^3 s^{-1})
np	1.988	10.632	1.102	9.969	1.962	10.561	1.110	10.001
npH (model I)	1.478	11.242	0.965	7.904	1.488	11.092	0.999	8.091
npH (model II)	1.539	10.823	1.096	8.538	1.491	11.040	1.022	8.159

FIG. 10. The mass-radius relation for neutron star sequences near the limiting mass for nucleons only (np) star (solid lines) and for stars with further inclusion of hyperons (npH) in the model II (dash-dotted lines). The results are for the models QMC (thick lines) and QHD (thin lines). The filled circles represent the maximum masses.

$1.44 M_\odot$ imposed by the larger mass of the binary pulsar PSR 1913 + 16 [46]. When hyperons are included, the central densities reached for all the stars above this lower mass limit suggest that the inner cores of these stars are rich in hyperons.

Constraints on the high density EOS can be derived from the measurement of the absolute upper limit to the rotation velocity Ω_{max} of a neutron star. This is possible because the maximum angular velocity of rotating neutron stars, in general, is an increasing function of the softness of the EOS which corresponds to more compact stars with high central densities and smaller equatorial radius. The maximum rotation rate of a neutron star is determined by the condition that the equatorial surface velocity equals the Keplerian velocity—the orbital velocity of a particle at the equator. At the Keplerian frequency, the rotating star is unstable with respect to mass shedding from the equator. In reality, the rotation may be more severely limited by gravitational radiation instability to nonaxisymmetric perturbations [47]. However, this instability has been later shown to be stabilized by the existence of the viscosity of stars at homogeneous density [48]. Therefore, the Keplerian rate may be considered as a reasonable estimate of the maximum rotation rate of a neutron star. The calculation of the Keplerian velocity for a given EOS is quite involved and has to be performed with full general relativity. On the other hand, a precise universal empirical formula was found by Haensel and Zdunik [49] for the maximum angular frequency Ω_{max} for rigid rotation in terms of maximum mass and radius of a nonrotating star for a given EOS:

$$\Omega_{max} = \mathcal{C}_\Omega (M_{max}/M_\odot)^{1/2} (R_{M_{max}}/10 \text{ km})^{-3/2} \text{ s}^{-1},$$

where M_{max} and $R_{M_{max}}$ are the maximum mass and corresponding radius of the nonrotating star. The dimensionless phenomenological constant independent of the EOS was found [49] to be $\mathcal{C}_\Omega = 7750$. Later calculations within the full framework of general relativity have shown [50] that this formula has an accuracy better than 5% for a wide range of realistic EOS which are both causal and stiff enough to support observed maximum mass $M_{max} = 1.44 M_\odot$. Since rotational energy stabilize a star, the most massive rotating star has more mass and radius than the maximum mass and radius of the corresponding nonrotating star. For our present equations of state, the Keplerian frequencies obtained by using the above formula are given in Table III for the respective rotating stars. It is observed that Ω_{max} closely follow the trend of the masses (and radii) of different models with the nucleons only star having the largest rotation rate and stars with hyperons in model I are the slowest. As mentioned above, this may be attributed to the smallest mass and thereby largest radius due to small gravitational attraction in the softest equation of state and vice versa.

V. SUMMARY AND CONCLUSION

In this paper we have investigated the effects of the internal quark structure of baryons on the neutron star properties within the relativistic mean-field quark-meson coupling model. This model describes baryons as nonoverlapping MIT bags in which the quarks interact through scalar and vector mean fields. Before any reliable prediction of the quark structure effects on neutron star properties at high densities can be made, it is essential that the QMC model reproduces at around nuclear matter densities the results of more established quantum hadrodynamics model where the relevant degrees of freedom are the structureless baryons. In the original QMC model, the bag constant was fixed at the free space value as a consequence of which the model predicts much smaller attractive scalar potential and hence smaller spin-orbit potential compared to the experimental results and that obtained in the QHD model. By considering a medium- (density-) dependent bag constant parametrized through direct coupling to the scalar field, correct spin-orbit splitting was observed. Moreover, this medium modified QMC model is found to be in excellent agreement with the low and moderate density results of QHD model with a general nonlinear scalar potential when both the models are calibrated to produce the same nuclear matter saturation properties. This improved fit is obtained by employing a bag constant which is a decreasing function of density, which however implies an increasing bag radius. We are therefore faced with the problem that due to the increasing bag radius and thereby overlapping bags the QMC model may not be applicable at the high density regime relevant to central densities of massive stars. A natural test of the reliability of the model at high densities then lies in the fact that the equation of state should be well-behaved and continuous when extrapolated to the extremes of density. Indeed, we have found that the physical observables exhibit reasonable behavior without any discontinuity at high densities up to $n_B \approx 10 n_0$ studied here. The deviation of the results observed at high densities in the two

effective field theoretical models, the QMC and QHD, with different underlying basic constituents may be interpreted as primarily arising from the crucial effects of the quark structure. The original version of the QMC model, where the important effect of quark-quark correlation associated with overlapping bags is neglected, exhibited discontinuity and therefore could not be extrapolated to high densities. A direct coupling of the bag constant to the scalar field is equivalent to higher powers of (nonlinear) scalar interactions. According to the modern viewpoint of effective field theory, higher order meson interaction includes the effect of correlations. Therefore, by employing a medium- (scalar-field-) dependent bag constant, we not only could reproduce the correct scalar potential but could also mimic the quark-quark correlations leading to a well-behaved EOS at high densities.

We have included two additional (hidden) strange mesons which couple only to strange quarks in a baryon bag in the QMC model and to hyperons in the QHD model. The rather strong hyperon-hyperon interaction can be accounted by these mesons. The coupling constants of the quarks and hyperons have been fixed by SU(6) symmetry relations based on quark-counting argument. The strange mesons are found to have considerable influence on the composition and structure of neutron star matter with hyperons. In absence of these mesons, the model QMCI exhibits softer EOS with smaller maximum mass star and larger corresponding radii than that in QHDI. With the inclusion of strange mesons, the additional attraction imparted by the scalar meson σ^* causes a drop in the effective masses of hyperons, the decrease being

determined by the number of strange quarks in the baryons. However, the two mesons (σ^*,ϕ) has an overall repulsive effect so that the EOS in the model II is stiffer compared to model I without the strange mesons. The repulsion is maximum in QMCII because of the decreasing in-medium scalar-baryon coupling constant and smaller scalar field σ^* than in QHDII. Consequently, the EOS in QMCII is significantly stiffened (and even stiffer than QHDI) with relatively larger maximum mass star and corresponding smaller radius. As observed in previous studies, the EOS is found to be considerably softened by incorporating hyperons as the new degrees of freedom which appear at $n_B \approx 2n_0$. The center of massive stars are found with comparable abundance of hyperons and nucleons; the strangeness fraction of stars in QMC models are relatively higher than in QHD models because of enhanced Ξ production. Rapid cooling by direct URCA process of all these stars are found to be dominated by nucleons due to large proton fraction ($Y_p \gtrsim 0.15$), the hyperons add only $\sim 5\%$ to this more dominant process. It therefore seems difficult to differentiate stars in the different models studied here with and without hyperons by a rapid cooling procedure.

[1] A. Burrows and J.M. Lattimer, Astrophys. J. **307**, 178 (1986).
[2] B. Friedman and V.R. Pandharipande, Nucl. Phys. **A361**, 502 (1981).
[3] R.B. Wiringa, V. Fiks, and A. Fabrocini, Phys. Rev. C **38**, 1010 (1988).
[4] B.D. Serot and J.D. Walecka, Adv. Nucl. Phys. **16**, 1 (1986); B.D. Serot, Rep. Prog. Phys. **55**, 1855 (1992).
[5] S.A. Chin, Ann. Phys. (N.Y.) **108**, 301 (1977).
[6] P.-G. Reinhard, Rep. Prog. Phys. **52**, 439 (1989).
[7] B.D. Serot and J.D. Walecka, Int. J. Mod. Phys. E **6**, 515 (1997).
[8] R.J. Furnstahl, C.E. Price, and G.E. Walker, Phys. Rev. C **36**, 2590 (1987).
[9] A.R. Bodmer and C.E. Price, Nucl. Phys. **A505**, 123 (1989).
[10] Y.K. Gambhir, P. Ring, and A. Thimet, Ann. Phys. (N.Y.) **198**, 132 (1990).
[11] N.K. Glendenning, Astrophys. J. **293**, 470 (1985); Phys. Rev. D **46**, 1274 (1992).
[12] R. Knorren, M. Prakash, and P.J. Ellis, Phys. Rev. C **52**, 3470 (1995).
[13] J. Schaffner and I.N. Mishustin, Phys. Rev. C **53**, 1416 (1996).
[14] M. Prakash, I. Bombaci, M. Prakash, P.J. Ellis, J.M. Lattimer, and R. Knorren, Phys. Rep. **280**, 1 (1997).
[15] D. Bandyopadhyay, S. Chakrabarty, and S. Pal, Phys. Rev. Lett. **79**, 2176 (1997).
[16] M. Arneodo, Phys. Rep. **240**, 301 (1994).
[17] Y. Nambu and G. Jona-Lasinio, Phys. Rev. **122**, 345 (1961); **124**, 246 (1961).
[18] P.A.M. Guichon, Phys. Lett. B **200**, 235 (1988).
[19] S. Fleck, W. Bentz, K. Shimizu, and K. Yazaki, Nucl. Phys. **A510**, 731 (1990).
[20] K. Saito and A.W. Thomas, Phys. Lett. B **327**, 9 (1994).
[21] A.W. Thomas, A. Michels, A.W. Schreiber, and P.A.M. Guichon, Phys. Lett. B **233**, 43 (1989); K. Saito, A. Michels, and A.W. Thomas, Phys. Rev. C **46**, R2149 (1992).
[22] K. Saito and A.W. Thomas, Phys. Lett. B **335**, 17 (1994); **363**, 157 (1995); Phys. Rev. C **51**, 2757 (1995); **52**, 2789 (1995).
[23] H.Q. Song and R.K. Su, Phys. Lett. B **358**, 179 (1995).
[24] X. Jin and B.K. Jennings, Phys. Lett. B **374**, 13 (1996).
[25] X. Jin and B.K. Jennings, Phys. Rev. C **54**, 1427 (1996).
[26] P.A.M. Guichon, K. Saito, E. Rodionov, and A.W. Thomas, Nucl. Phys. **A601**, 349 (1996); K. Saito, K. Tsushima, and A.W. Thomas, Phys. Rev. C **55**, 2637 (1997); **56**, 566 (1997).
[27] P.G. Blunden and G.A. Miller, Phys. Rev. C **54**, 359 (1996).
[28] H. Müller and B.K. Jennings, Nucl. Phys. **A640**, 55 (1998).
[29] K. Tsushima, K. Saito, J. Haidenbauer, and A.W. Thomas, Nucl. Phys. **A630**, 691 (1998).
[30] J. Boguta and A.R. Bodmer, Nucl. Phys. **A292**, 413 (1977); J. Boguta and H. Stöcker, Phys. Lett. **120B**, 289 (1983).
[31] J. Schaffner, C.B. Dover, A. Gal, D.J. Millener, C. Greiner,

and H. Stöcker, Ann. Phys. (N.Y.) **235**, 35 (1994).

[32] R.E. Chrien and C.B. Dover, Annu. Rev. Nucl. Part. Sci. **39**, 113 (1989).

[33] C. Adami and G.E. Brown, Phys. Rep. **234**, 1 (1993).

[34] M. Asakawa and K. Yazaki, Nucl. Phys. **A504**, 668 (1989); M. Lutz, S. Klimt, and W. Weise, **A542**, 521 (1992).

[35] R. Alkofer, H. Reinhardt, and H. Weigel, Phys. Rep. **265**, 139 (1996).

[36] M.K. Banerjee, Phys. Rev. C **45**, 1359 (1992); V.K. Mishra, *ibid.* **46**, 1143 (1992); E. Naar and M.C. Birse, J. Phys. G **19**, 555 (1993).

[37] R.J. Furnstahl, B.D. Serot, and H.-B. Tang, Nucl. Phys. **A598**, 539 (1996); **A618**, 446 (1997).

[38] H. Müller and B.D. Serot, Nucl. Phys. **A606**, 508 (1996).

[39] H. Müller and B.K. Jennings, Nucl. Phys. **A626**, 966 (1997).

[40] G.E. Brown, S. Klimt, M. Rho, and W. Weise, Z. Phys. A **331**, 139 (1988).

[41] J.M. Lattimer, C.J. Pethick, M. Prakash, and P. Haensel, Phys. Rev. Lett. **66**, 2701 (1991); C.J. Pethick, Rev. Mod. Phys. **64**, 1133 (1992).

[42] M. Prakash, M. Prakash, J.M. Lattimer, and C.J. Pethick, As-

trophys. J. Lett. **390**, L77 (1992).

[43] S. Chandrasekhar, *Hydrodynamic and Hydromagnetic Stability* (Dover, New York, 1969), p. 583.

[44] G.B. Cook, S.L. Shapiro, and S.A. Teukolsky, Astrophys. J. **398**, 203 (1992).

[45] R.C. Tolman, Phys. Rev. **55**, 364 (1939); J.R. Oppenheimer and G.M. Volkoff, *ibid.* **55**, 374 (1939).

[46] J.M. Weisberg and J.H. Taylor, Phys. Rev. Lett. **52**, 1348 (1984).

[47] S. Chandrasekhar, Phys. Rev. Lett. **24**, 61 (1970).

[48] L. Lindblom and S.L. Detweiler, Astrophys. J. **211**, 565 (1977); J.L. Friedman, J.R. Ipser, and L. Parker, *ibid.* **304**, 115 (1986); Phys. Rev. Lett. **62**, 3015 (1989); R.F. Sawyer, Phys. Rev. D **39**, 3804 (1989).

[49] P. Haensel and J.L. Zdunik, Nature (London) **340**, 617 (1989).

[50] J.L. Friedman and J.R. Ipser, Philos. Trans. R. Soc. London, Ser. A **340**, 391 (1992); J.M. Lattimer, M. Prakash, D. Masak, and A. Yahil, Astrophys. J. **355**, 241 (1990); M. Salgado, S. Bonazzola, E. Gourgoulhon, and P. Haensel, Astron. Astrophys. **108**, 455 (1994); **291**, 155 (1994).